

Study of Shear and Pressure Flow on the Variation of Ship Hull Shapes as One of the Biofouling Growth Factors

Muhammad Auliya Alamsyah¹, Muhammad Luqman Hakim¹ and I Ketut Aria Pria Utama¹

¹*Department of Naval Architecture, Faculty of Marine Technology, Institut Teknologi Sepuluh Nopember (ITS), Jl. Arief Rahman Hakim, Surabaya, Indonesia*

Keywords: Ship Hydrodynamics, Biofouling, Marine Growth, Pressure and Shear Force Distribution.

Abstract: In this paper, the pattern of shear force distribution and pressure on two hull models are explained using the Computational Fluid Dynamics (CFD) numerical method. The two hull models are general cargo and barge hulls, where they are chosen because they have a significant hull shape difference, therefore the pattern of shear distribution and pressure force can be different. The difference in shear distribution and pressure force is one of the growth factors of biofouling, where biofouling is a problem on ships. Biofouling causes the hull of the ship to become rough and increase the resistance of the ship, resulting in a waste of energy and increase the number of emissions. From the results of this study it was found that the distribution of both is almost the same, namely the area that has the potential to be easily grown with biofouling (minimal shear force and maximum pressure), i.e. at the end of the bow and stern end, with only slight differences in pattern and.

1 INTRODUCTION

Biofouling is the accumulation of aquatic organisms such as microorganisms, plants, and animals that attached to surfaces and structures that wetted into the sea like ship hull and cause various problems (IMO, 2011). Problems arising from biofouling include: first, ecosystem damage through the spread of invasive species which then results in a decrease in fishery products and the emergence of a new epidemic of a disease; second, increasing ship resistance which lead to increased emissions which then have an impact on climate change and global warming as well as economic value that is lost in energy dissipation (Schultz, 2007; Turan, et al., 2016; Monty, et al., 2016; Utama, et al., 2017; Hakim, et al., 2017; Nugroho, et al., 2017; Hakim, et al., 2018).

Biofouling that attaches and grows at the hull of the ship causes the surface of the hull to become rough and consequently, it can increase the friction resistance (Schultz, et al., 2011). When there is an increase in resistance, the power requirements will increase, from this it can be said that energy dissipation occurs and leads to more emissions. IMO notes that emissions generated by ships around the world are 2.2% of total man-made emissions

worldwide in 2012 (IMO, 2015), and are predicted to increase by 50-250 percent by 2050 (IMO, 2009).

Keeping the ship's hull clean from biofouling can reduce emissions by up to 10% (ICCT, 2013; Molland, et al., 2014) where this is suggested by IMO through the Energy Efficiency Design Index (EEDI) (IMO, 2012). For this reason, it is necessary to use an anti-fouling system, such as the one that already exists, with anti-fouling coating and routine cleaning when dry docking. Unfortunately, the mechanisms of the anti-fouling coating are to release biocide compounds into the water, which according to Rompay (2012), it will eventually become a new problem for the marine environment in the future.

According to the results of an investigation and test from Hunsucker (2014) that the growth of biofouling on each part of the hull is not the same. Hunsucker (2016) also conducted an experiment to determine the effect of the hydrodynamic effect of shear stress on biofouling growth. The effects of static and dynamic conditions have also been observed on water conditions (Zargiel & Swain, 2014). The effect of ship speed on biofouling growth has also been observed by Coutts (2010). From their explanation that the hydrodynamic effect such as speed, shear stress, and pressure can affect the growth of biofouling in the hull of the ship.

Based on the results of the Hunsucker (2014) and Hunsucker (2016) research, this paper will discuss the pattern of shear stress and pressure distribution on the hull using numerical CFD method. As hull models, two different types of hulls are used, namely general cargo hull and barge hull. Both models were chosen because they have a significantly different of hull shape where the cargo hull has a more streamlined form than the barge.

2 PHYSICAL COMPONENTS OF MAIN HULL RESISTANCE

When the ship sails, it will get a drag from the fluid. The drag component can be divided into friction resistance, pressure resistance and residual resistance (wave). Friction resistance is strongly influenced by the hull roughness of the ship. While the pressure resistance and wave resistance are influenced by the shape of the hull of the ship. In general, the equation is written as follows:

$$R_T = R_F + R_{VP} + R_W \quad (1)$$

$$R_T = R_V + R_W \quad (2)$$

where R_T , R_F , R_{VP} , R_W , and R_V are total resistance, frictional resistance, viscous pressure resistance, wave resistance, and viscous resistance, respectively, (Molland, et al., 2011).

The difference for shear force and pressure can be seen in Figure 1, where the shear force (τ) is a force that is parallel to the wall or surface of the hull which is affected by fluid viscosity. meanwhile the pressure (P) is a force perpendicular to the surface of the shape from a ship hull.

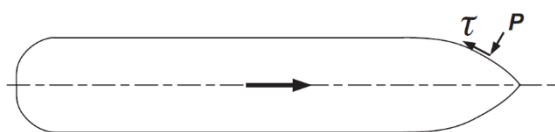


Figure 1: Frictional and pressure forces [22].

2.1 Shear Force

Friction drag is a part of the shear stress on the object wall and above that is affected in the area of the inner boundary layer. If the shape of the object is dominated by line form that is parallel to the upstream velocity, then the component of the shear force is dominant than the force of pressure. If the direction

of the resultant of the shear force arises in the opposite direction of the upstream velocity axis, then it contributes to the drag force, but if it is perpendicular then it contributes to the lift force.

Shear stress is obtained from the boundary layer velocity profile whether it is laminar or turbulent or transition as shown in Figure 2. From the graph of the velocity profile, the surface shear stress can be known by the following formula:

$$\tau_w = \mu \left[\frac{\partial u}{\partial y} \right]_{y=0} \quad (3)$$

where μ is the fluid dynamic viscosity and $\left[\frac{\partial u}{\partial y} \right]$ is the velocity gradient at the surface.

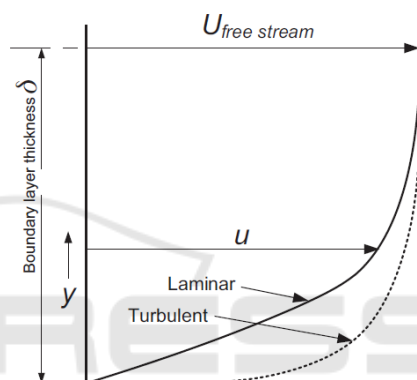


Figure 2: Boundary layer velocity profiles.

2.2 Pressure Force

Pressure force is the force generated due to the presence of fluid which is blocked by the wall of the object in the normal direction of the area (Molland, et al., 2011), as shown in Figure 1. While the pressure distribution on the vessel as shown in Figure 3.

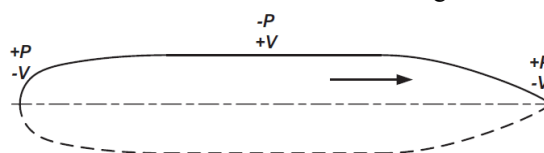


Figure 3: Pressure variations around a body of ship (Molland, et al., 2011).

3 THE PROCESS OF ATTACHING BIOFOULING

Biofouling is the accumulation of aquatic organisms such as microorganisms, plants, and animals on immersed surfaces and structures, including microfouling and macrofouling. Microfouling is the bacteria and diatoms and slimy substances produced, usually referred to as slime layers. Macrofouling is a large multicellular organism that can be seen by the human eye such as barnacles, tapeworms, or algae leaves (IMO, 2011). More than 4000 species of animals and plants are recorded as biofouling worldwide (Nair, 2013).

The process of attaching biofouling to the substrate immersed in the aquatic environment is explained by Nair (2013). After the structure is immersed, a first layer is formed consisting of bacteria, diatoms, algal spores, and detritus. The first layer is important because it affects macrofouling thereafter, as shown in Figure 4 (Nybakken, 1982). Then, the bacteria develop very quickly and form an important constituent in the first layer. The bacteria become firmly attached, and in just one hour the cells grow an average of 1-2 microns and continue to divide. This causes the population to increase twice every four hours. The bacterial colonies secrete polysaccharides, which make the surface of the film slimy and sticky and afterward make the algae stick. They also ensnare larvae, change the color of the surface, so as a place for food for macrofouling that comes afterward.

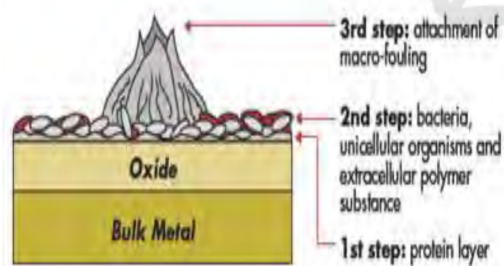


Figure 4: The process of attaching biofouling on metals.

In the process of attaching biofouling to a surface is influenced by many factors, so it is very difficult to determine the exact rules that can be used to determine where it will stick. Based on this uncertainty, the scientists tried to use the theory of opportunities for the biofouling attachment phase on the surface by considering the values of pressure, shear, and turbulence (Mullineaux & Garland, 1993).

In the attachment phase, there are two main requirements that must be fulfilled so that the biofouling attachment instincts can function properly. First, environmental disturbances (shear stress and turbulence) are low. Second, biofouling organisms must have good mobility. The first requirement will guide biofouling organism's instincts to select attachment areas with minimum disturbances, and the second requirement serves to serve the instincts to move attached (Mullineaux & Garland, 1993).

Based on information obtained by biofouling organism instincts, the priority will be placed on the relatively quiet attachment area. From the explanation above, it can be predicted that the intensity of attachment in areas that have low hydrodynamic intensity will have a greater chance of attachment compared to areas that have high hydrodynamic intensity.

In the biofouling growth phase, there are three main factors that influence the growth process. The three processes include the supply of food ingredients, food filtration mechanisms and food digestion. If the hydrodynamic conditions support the above three processes, then the growth will take place optimally. Distribution of food ingredients along with other living substances will be difficult to take place due to turbulent flow. The next factor that affects the growth process is filtering food ingredients. If the screening process takes place effectively, more food will be obtained. Most biofouling organisms that live (statically) use a filtering method to get their food. This filter is in the form of antennas which are equipped with fine hairs to filter the food ingredients dissolved in the water and enter into the mouth (Pascual, 1992).

The explanation above explains that the hydrodynamic characteristics affect the biofouling growth process. The hydrodynamic factors include: patterns of the tendency to speed, pressure and surface shear stress and turbulence.

4 MODELS

The hull models of the cargo ship and barge used for this study were made to have the same size as described in Table 1. From the table, it can be seen that the value of WL Length, Breadth (B) and Draught (T) have the same value, whereas the different are Displacement, WSA, and Cb, where the barge has a higher value.

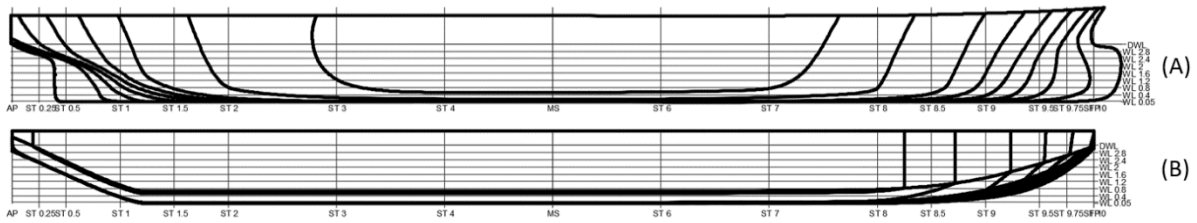


Figure 5: Sheer plan of (A) General Cargo and (B) Barge.

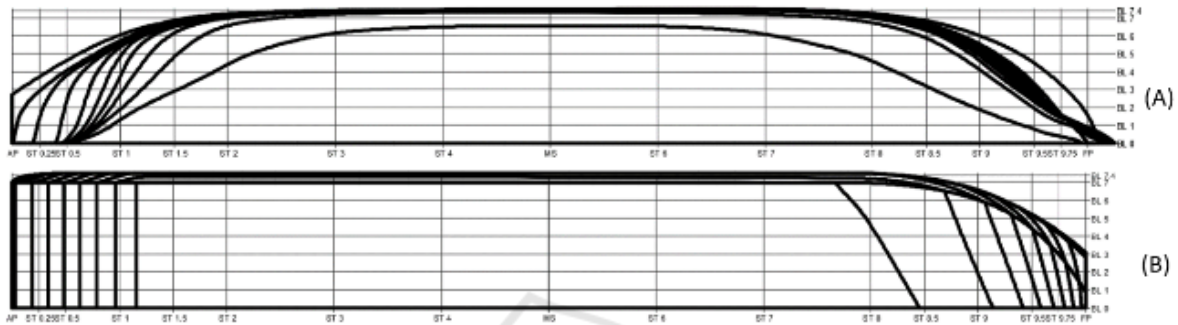


Figure 6: Half breadth plan (A) General Cargo and (B) Barge.

Table 1: This caption has one line so it is centered.

Item	Barge	Cargo	Units
Displacement	2569	2364	ton
WL Length	60	60	m
B	15	15	m
T	3.2	3.2	m
WSA	1187	1092	m ²
Cb	0.87	0.8	-
LCB %	48.97	51.05	%

To find out how different the hull shape of the general cargo and barge model used in this study can be seen in Figure 7 for the general cargo body plan and in Figure 8 for the barge. Then the shape of the sheer plan and half breadth plan can be seen in Figure 5 and Figure 6 respectively.

In this analysis, the roughness model of biofouling is not carried out. The surface of the two models is made smooth. Because the purpose of this analysis is to compare the effects of different hull forms on shear stress distribution and pressure force as one of the biofouling growth factors on a ship.

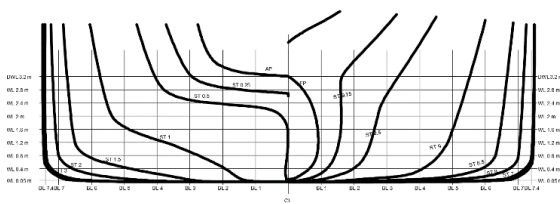


Figure 7: Body plan of General Cargo.

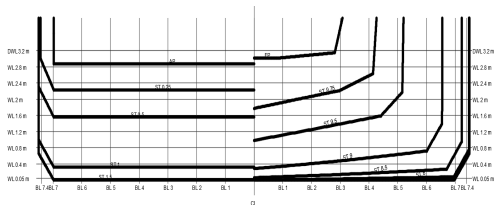


Figure 8: Body plan of General Cargo.

5 NUMERICAL METHODS

In this analysis, the results needed are only viscous and pressure value, so the domain and boundary condition set applied are one fluid computation, or without taking into account the effects of wave resistance.

The size of the domain and boundary condition in the numerical model of this study can be seen in Figure 9. In the Figure 9, it can also be seen the quality of the mesh generation used. the number of elements in this calculation is around 6 million elements and has met the convergence criteria. Then the turbulence model used is k- ω -SST, with the second order computation method and residual targets up to 10⁻⁴.

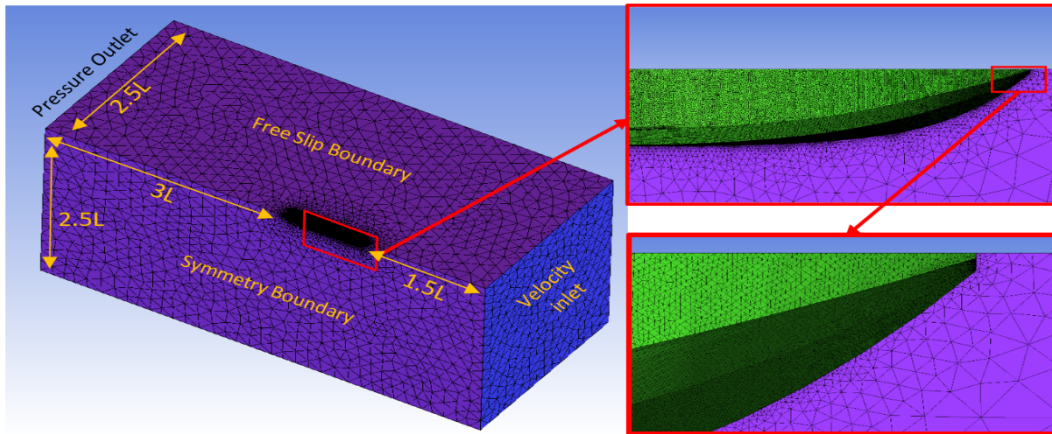


Figure 9: Domain computation and mesh generation.

In this numerical modeling, velocity variations have been carried out just for 5 knots and 10 knots. Because the author believes that the pattern of shear stress distribution and surface pressure due to differences in speed does not change, but what changes is only the value. Therefore, in this simulation, the velocity of 5 knots and 10 knots are chosen.

6 RESULT AND DISCUSSION

6.1 Grid Sensitivity Test

To get the optimal mesh size so that the calculation results from the model are close to the true value and are still within computer capabilities, a grid sensitivity test is performed. The result of the test can be seen in Figure 10, where from the result the number of elements that can be used in computing is around 6 million elements because the calculation results for the number of elements 6 million and 13 million only have a difference under 2%.

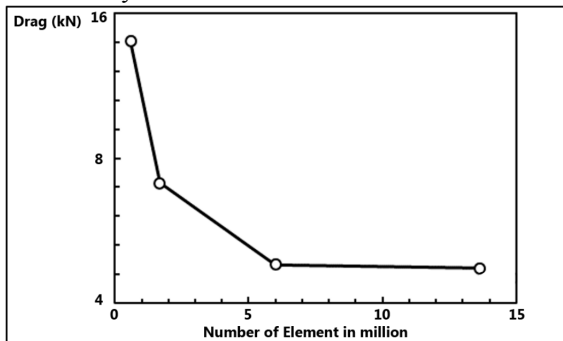


Figure 10: Result of grid sensitivity test.

6.2 Validation Study

Validation of this analysis is comparing the result from numerical method with empirical method. The CFD results of the two models is compared with Holtrop [27] as empirical calculation method. Based on the calculation of the resistance in formula 1 and formula 2, if it is changed in the form of a coefficient it will become:

$$C_T = C_V + C_W \quad (4)$$

Where C_T , C_V , and C_W are total drag coefficients, viscous resistance coefficients, and wave resistance coefficients, respectively.

Table 2: Comparison of computed RV values between numeric and empiric.

Speed	5 knots					ΔR_V (%)
	Method	Holtrop				
	R_V	R_T	C_V	C_W	R_V	
Barge	13,46 6	16,65 7	3,20 0	0,51 3	14,35 6	-6%
Cargo	10,10 9	13,00 5	2,86 3	0,10 8	12,53 2	- 19%
Speed	10 knots					ΔR_V (%)
Method	Holtrop					
	R_V	R_T	C_V	C_W	R_V	
Barge	50,05 1	68,10 0	2,93 7	0,73 8	54,42 4	-8%
Cargo	37,21 6	54,47 4	2,60 1	0,54 0	45,10 9	- 17%

By using numerical CFD modeling with the method in this case, the viscous resistance (R_V) values for each model will be obtained for speeds of 5 knots and 10 knots. Then the value is compared with the results of the Holtrop empirical calculation for both models and at the same speed. The results of the comparison can be seen in Table 2, where the results can be said to be quite valid.

6.3 Shear Stress Distribution

In all the results plots illustrated in this paper are the simulation results with a speed of 5 knots. The speed of 10 knots is not displayed because the result of the distribution pattern is the same as the result of the speed of 5 knots, which is different only the value.

The results of the shear force distribution pattern are shown in Figure 11 and Figure 12. The results show that the distribution pattern on the two hull models is different.

For the results of the general cargo, hull model plotted on the rear and front view in Figure 11A and B (body plan), the smallest shear force is at the front and rear with a value of less than 2 Pa. For the front (see Figure 11 B) it is around the bulbous bow area slightly up with a small area. While on the afterward (see Figure 11 A), it occurs in the stern bow area upwards with extended area until the end. In this area, it can be said that disruption due to shear force to biofouling growth is minimal.

Still, with the general cargo model, the highest shear force value occurs in the hull curve which will lead to the propeller area and the curve after the bulbous bow. In that area, the shear force is 5 times higher, 10 Pa. Therefore, in this area biofouling gets

the biggest disturbance from the influence of the shear force. For more details about the distribution of the shear force pattern can be seen in Figure 12 A and B as the appearance of the side and bottom view to get a longitudinal view.

In Figures 11 C D and 12 C D, they are the shear force distribution pattern for barge model. The highest shear force value is at the back, which is the meeting area between the parallel middle body and the stern. Then at the front, there is shear force value that is not as high as general cargo model, only with a value of around 8 - 9 Pa but with a wider area. In this area, biofouling growth has a higher disturbance.

Then the lowest shear force value on the barge occurs at the end of the bow and the stern end is almost similar to general cargo but with a slightly wider area. In this area, biofouling receives the least interference from the shear force effect.

6.4 Pressure Distribution

The computational results for the distribution of pressure forces on both models can be seen in Figures 13 and 14. From the results of calculations on both models also obtained a different pressure distribution pattern. If shear force interferes with the biofouling growth process, it is different from the pressure force. The force of pressure can help biofouling stick to the hull more easily.

The two models have almost the same distribution pattern, which is at the fore and after ends as described in Figure 3 above. At general cargo, the

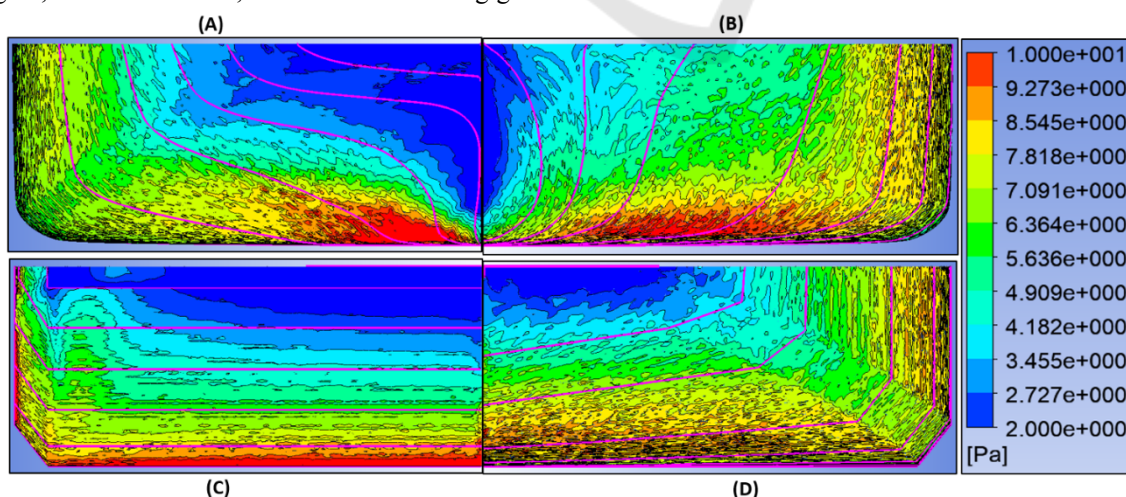


Figure 11: Shear stress distribution: (A) back view of General Cargo, (B) front view of General Cargo, (C) back view of Barge, and (D) front view of Barge

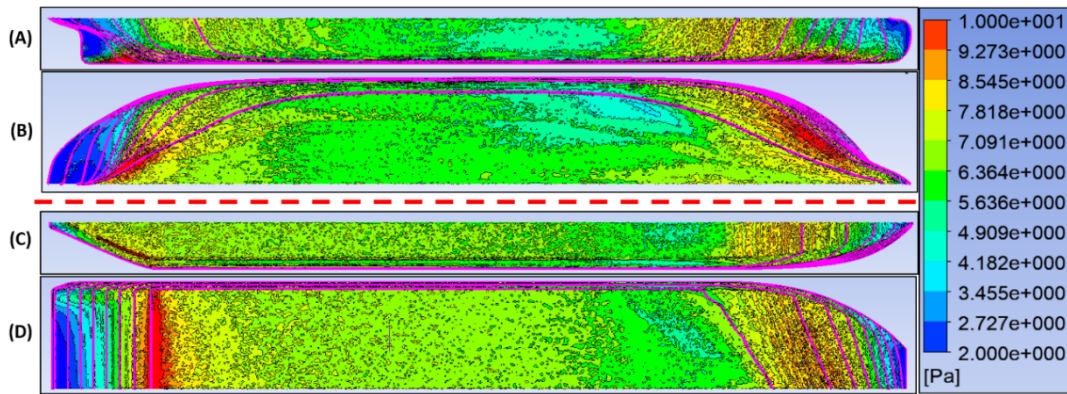


Figure 12: Shear stress distribution: (A) side view of General Cargo, (B) bottom view of General Cargo, (C) side view of Barge, and (D) bottom view of Barge.

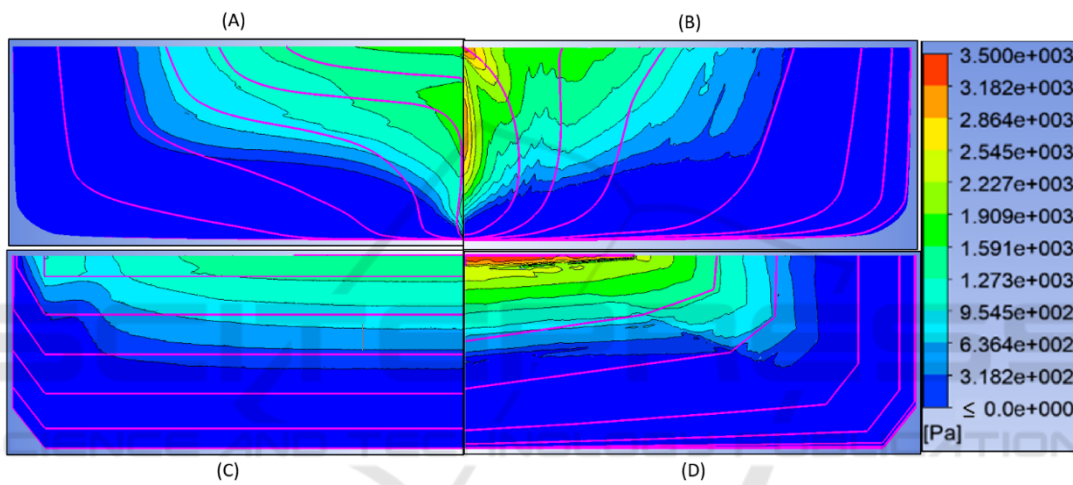


Figure 13: Pressure force distribution: (A) back view of General Cargo, (B) front view of General Cargo, (C) back view of Barge, and (D) front view of Barge

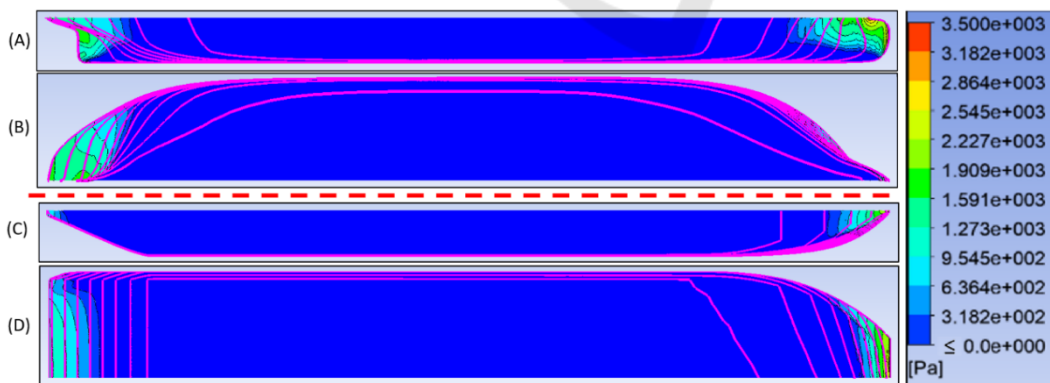


Figure 14: Pressure force distribution: (A) side view of General Cargo, (B) bottom view of General Cargo, (C) side view of Barge, and (D) bottom view of Barge.

highest pressure is at the end of the bulbous bow and stern after the propeller, while the barge also occurs at the end of the bow and the stern area. These areas

are areas where the shear force value is weak, so biofouling can be found more often in this area.

Then for at the middle hull, both have pressure with very small to negative values as shown in Figure 14 in color of blue. In this area, biofouling is more difficult to stick to than the front and rear areas of the stomach.

7 CONCLUSIONS

One way to reduce emissions on ships is to maintain the hull clean of biofouling by using an anti-fouling system or cleaning when docking. Biofouling can grow in the hull of the ship with various factors, one of which is the hydrodynamic characteristics of water flow such as shear and pressure force. On ships, the distribution of shear and pressure forces are influenced by the hull shape of the ship itself.

From the results of this study, the distribution of shear and pressure forces was obtained for general cargo and barge hulls. The distribution of both is almost the same, namely an area that has the potential to be easily grown with biofouling (minimal shear force and maximum pressure), ie at the end of the arc and the tip of the stern, with only slight differences in patterns, values, and extent. Subsequent suggestions need to be taken into account other influential factors such as speed, type, and quality of anti-fouling, operating patterns, and other hull forms.

REFERENCES

- Coutts, A. D. et al., 2010. Effect of Vessel Voyage Speed on Survival of Biofouling Organisms: Implications for Translocation of Non-indigenous Marine Species. *Biofouling*, Volume 26 No. 1, pp. 1-13.
- Hakim, M. L. et al., 2018. *Assessment of Drag Penalty Resulting from the Roughness of Freshly Cleaned and Painted Ship-Hull Using Computational Fluid Dynamics*. 11th International Conference on Marine Technology (UTM). Kuala Lumpur.
- Hakim, M. L. et al., 2018. *Investigation of Fuel Consumption on an Operating Ship Due to Biofouling Growth and Quality of Anti-Fouling Coating*. The First Maluku International Conference on Marine Science and Technology (Unpatti). Ambon.
- Hakim, M. L. et al., 2017.. *Review of Correlation between Marine Fouling and Fuel Consumption on A Ship*. SENTA: 17th Conference on Marine Technology (ITS). Surabaya.
- Holtrop, J. & Mennen, G., 1978. A Statistical Power Prediction Method. *International Shipbuilding Progress*, Volume 25.
- Hunsucker, J. T., Hunsucker, K. Z., Gardner, H. & Swain, G., 2016. Influence of Hydrodynamic Stress on the Frictional Drag of Biofouling. *Biofouling*, Volume 32 No. 10, pp. 1209-1221.
- Hunsucker, K. Z., Kokaa, A., Lundb, G. & Swain, G., 2014. Diatom Community Structure on In-service Sruise Ship Hulls. *Biofouling*, Volume 30 No. 9, p. 1133-1140.
- ICCT, 2013. *Long-Term Potential for Increased Shipping Efficiency Through the Adoption of Industry-Leading Practices*. International Council on Clean Transportation. Washington.
- IMO, 2009. *Second IMO GHG Study 2009*. International Maritime Organization. London.
- IMO, 2011. *Guidelines for The Control and Management of Ships Biofouling, Resolution MEPC.207 (62)*. s.l.:Marine Environment Protection Committee. London.
- IMO, 2012. *Guidelines on Survey and Certification of the Energy Efficiency Design Index (EEDI) MEPC 214 (63)*. s.l.:Marine Environment Protection Committee. London.
- IMO, 2012. *Guidelines on the Method of Calculation of the Attained Energy Efficiency Design Index (EEDI) for new ships MEPC.212 (63)*. s.l.:Marine Environment Protection Committee. London.
- IMO, 2015. *Third IMO GHG Study 2014*. International Maritime Organization. London.
- Molland, A., Turnock, S. & Hudson, D., 2011. *Ship Resistance and Propulsion*. Cambridge University Press. Cambridge.
- Molland, A., Turnock, S., Hudson, D. & Utama, I., 2014. Reducing Ship Emissions: A Review of Potential Practical Improvements in The Propulsive Efficiency of Future. *International Journal of Maritime Engineering*, Volume 156 A2, pp. 175-188.
- Monty, J. P. et al., 2016. An Assessment of the Ship Drag Penalty Arising from Light Calcareous Tubeworm Fouling. *Biofouling*, Volume 32 (4), pp. 451-464.
- Mullineaux, S. Y. & Garland, E. D., 1993. Larva Recruitment in Response to Manipulated Filed Flows. *Marine Biology*, Volume 116.
- Nair, N. U., 2013. *Marine Fouling and Control Measures Cochin: Former Scientist Emeritus (ICAR)*. s.l.:Central Institute of Fisheries Technology. Kochi, India.
- Nugroho, B. et al., 2017. *In-situ Turbulent Boundary Layer Measurements over Freshly Cleaned Ship-Hull under Steady Cruising*. International Conference on Ship and Offshore Technology (RINA). Jakarta.
- Nybakken, J., 1982. *Biologi Laut : Suatu Pendekatan Ekologis*. Gramedia. Jakarta.
- Pascual, C., 1992. Small Scale Turbulence on Zooplankton Metabolism Affect Torbulence on Heartbeat Rates Planktonic Crustacean. *Marine Biology*, Volume 124.
- Rompay, B. V., 2012. *Surface Treated Composites White Book*. Tahoka Press. Clearwater, FL.
- Schultz, M. P., 2007. Effects of Coating Roughness and Biofouling on Ship Resistance and Powering. *Biofouling*, Volume 23 (5), pp. 331-341.
- Schultz, M. P., Bendick, J. A., Holm, E. R. & Hertel, W. M., 2011. Economic Impact of Biofouling on A Naval Surface Ship. *Biofouling*, Volume 27, pp. 87-89.

- Turan, O., Demirel, Y. K., Day, S. & Tezdogan, T., 2016. Experimental Determination of Added Hydrodynamic Resistance Caused by Marine Biofouling on Ships. *Transportation Research Procedia*, Volume 14, pp. 1649-1658.
- Utama, I. K. A. P. et al., 2017. *A Study of Skin Friction-Drag from Realistic Roughness of a Freshly Cleaned and Painted Ship Hull*. International Symposium on Marine Engineering (ISME). Tokyo.
- Zargiel, K. A. & Swain, G. W., 2014. Static vs Dynamic Settlement and Adhesion of Diatoms to Ship Hull Coatings. *Biofouling*, Volume 30 No. 1, pp. 115-129.

